CrossMark

The effect of barrier layer conditions on the electrodeposition efficiency and magnetic properties of Fe nanowire arrays

S. F. Akhtarianfar[1] · **A. Ramazani[1,2]** · **M. Almasi-Kashi[1,2]** · **A. H. Montazer[1]**

Abstract

Fabrication of different nanostructures based on template-assisted methods has become conventional, due to their numerous potential applications. In this paper, Fe nanowire arrays (NWAs) were fabricated using a pulsed electrodeposition in porous anodic alumina (PAA) templates. The effect of alumina barrier layer conditions such as barrier layer temperature (BLT) and Cu pre-plating at the dendritic sections of pores on the electrodeposition efficiency (EE) and magnetic properties of Fe NWs in two pH regimes (2.6 and 4.0) has been investigated. At pH 4.0, BLT was changed from ~ 4 to ~ 32 °C, leading to an EE of approximately 60% for BLT ~ 24 °C. Moreover, to overcome the problem of low EE ~ 2% at the pH of 2.6, Cu pre-plating was performed with deposition current densities of 25 and 35 mA/cm². This procedure increased the EE up to about 40%, providing a promising approach to enhance the EE in the fabrication of Fe NWAs. Furthermore, a nearly constant trend of magnetic properties was observed for highly crystalline Fe NWs.

Abbreviations

NWAs	Nanowire arrays
PAA	Porous anodic alumina
BLT	Barrier layer temperature
EE	Electrodeposition efficiency
M_s	Saturation magnetic moment

1 Introduction

Recently, nanotechnology has become an increasingly active area of research for scientists because of its tremendous economic potential. Among different kinds of nanostructures, magnetic nanostructured materials have attracted considerable attention due to their applications in high-density storage devices, field emission displays, and also biological, chemical and magnetic sensors [1–4]. Numerous effective methods have been devised to fabricate magnetic nanostructures (composed of elements and compounds Fe, Co, Ni, CoFe, NiFe, etc.) such as electron beam lithography [5–8], X-ray lithography [9], interference lithography [10, 11], nanoimprint lithography [12], sputtering [13], and chemical vapor deposition [14]. One of the most convenient and cost-effective methods within the mentioned approaches is the template-based technique which is widely used to produce highly ordered magnetic nanowires (NWs) [15, 16].

Porous anodic alumina (PAA) has been raised as a technically feasible template, because its fabrication process is not complex and does not need expensive technology [16, 17]. Fabrication of PAA which is performed during a process called aluminum anodization leads to a relatively thick alumina layer between aluminum substrate and the bottom of nanopores. This dielectric layer named "barrier layer" (BL) limits the reduction of cations in the electrochemical solution to form magnetic NWs [18–20]. To overcome this challenge, various electrodeposition approaches have been reported including direct current (DC), alternating current (AC), and pulsed electrodeposition (PED). DC electrodeposition is a complicated and time-consuming process due to the insulating nature of BL and its high electrical resistivity. In AC and PED deposition methods which are simple and industrially scalable, BL is not entirely removed and electrodeposition is performed in the presence of BL. A process called "barrier layer thinning" is used after anodization to reduce the high electrical resistivity of BL [16]. Thus, precise controlling of the BL plays a major role in electrodeposition of different materials into the pores and fabricating magnetic NWs.

✉ S. F. Akhtarianfar
farshad.akhtarian@gmail.com

1 Institute of Nanoscience and Nanotechnology, University of Kashan, Kashan 87317-51167, Iran

2 Department of Physics, University of Kashan, Kashan 87317-51167, Iran

For this reason, many studies have been performed to accurately manipulate the BL for optimizing electrodeposition efficiency (EE) and magnetic properties of NWs. The effect of BL thickness (δ_b) on the fabrication of Ni NW arrays (NWAs) has been reported elsewhere [31]. It was demonstrated that the best %EE and NW homogeneity are obtained for $\delta_b \sim 10$ nm and slight deviations from this value lead to abrupt decrease in efficiency of electrodeposition [21]. In addition, it has been showed that the optimum value of BL thickness for the fabrication of Fe NWs is between 8 and 10 nm [22]. Besides BL thickness, the other effective parameter is BL's branched-shape structure which influences the growth of NWs. It was showed that, during BL thinning, branched-shape (tree-like) porous structures are created at the end side of each pore, contributing to the electrodeposition process [16, 23]. Therefore, it has been evidenced that filling the BL's dendritic structure with Cu (called pre-plating process) before the growth of Co NWAs has a substantial effect on the corresponding magnetic properties [24]. In addition to BL study, the effect of other parameters such as current density, deposition temperature, voltage, pH value, electrolyte concentration, pulse shape, and pulse relaxation time on the growth of NWs has also been investigated [25–34]. Specifically, for the deposition of Fe NWAs, the effects of the mentioned factors have been optimized, according to the literature [22, 35, 36].

In this paper, we introduce a fabrication parameter named "barrier layer temperature" (BLT) which highly affects the BL conditions of PAA template. We report the effect of this parameter and also Cu pre-plating at the dendritic sections of pores on the EE and magnetic properties of Fe NWAs. In two pH regimes, an experimental setup was applied to change BLT ranging between ~4 and 32 °C.

2 Experimental details

Before performing a two-step anodizing process (mild anodization) for fabrication of PAA template, ultra-pure (99.999% purity) aluminum disc purchased from Alfa Aesar with a working area of 0.78 cm^2 was degreased and rinsed in acetone, ethanol, and distilled water and then electropolished with the mixture of perchloric acid and ethanol (volume ratio 1:4). All the chemicals were analytical grade and used as received without further purification. The electropolishing process was performed with the aforementioned solution at 10 °C under the voltage of 20 V during 180 s [37, 38]. Next, mild anodization was accomplished using 0.3 M oxalic acid and a constant voltage of 40 V at 17 °C with an accuracy of ± 0.1 °C, so that the duration of the first and second steps was 5 and 4 h, respectively [30].

During the anodization process, the oxide BL is formed and separates parallel hexagonal-close-packed nanopores

(perpendicular to the Al surface) from aluminum metal. The porous structure evolution results from the dynamic equilibrium between the film growth at the aluminum–alumina interface and the field-assisted oxide dissolution at the oxide–electrolyte interface. Both Al^{3+} and O^{2-} are passed through the BL under the driving force of the electric field [39]. To make BL suitable for PED, it must be thinned, because BL is a rather thick and dielectric layer (thus allowing quantum electron tunneling to occur leading to a current flow through the alumina). Therefore, the mild anodization is followed by BL thinning in which anodization voltage V_a is exponentially decreased from 40 to 10 V based on the equation $V_{\text{thinning}}(t) = V_a \exp(-\eta t)$, where V_{thinning} is the thinning voltage and η is the parameter by which the rate of exponentially decreasing voltage is controlled ($\eta = 0.001$ s^{-1}). It has been showed that BL thickness is dependent on V_a [24, 40].

After preparing PAA template with thinned BL, the electrodeposition method was applied to fill the nanopores. In this study, two sets of samples have been fabricated. In the first set, the branched-shape structure at the pore bottom of each sample has been filled by Cu (pre-plating process) before electrodeposition of Fe NWAs. The electrolyte for Cu pre-plating and Fe electrodepositing into PAA was the mixture of 45 g/l boric acid (H_3BO_3) and 0.3 M $CuSO_4.5H_2O$ and $FeSO_4.7H_2O$, respectively. Acidity (pH) value of Fe electrolyte solution was adjusted to 2.6 and 4.0 [41, 42]. In other words, the electrodeposition of Fe NWs was performed in two acidity regimes, while the acidity of electrolyte for Cu deposition was constant to 3.5. The temperature of the electrodeposition solution was 30 °C and remained constant during the process, whereas the barrier layer temperature of each sample was mainly set into three different temperatures: 8, 16, and 24 °C.

An experimental setup was designed and built to control both BLT and electrolyte temperature at the same time. Figure 1 displays the operation of this system schematically. The BL cooling mechanism is based on the high conductivity of aluminum which is about 205 W/(m K) at room temperature. Therefore, cooling of aluminum by a temperature controller leads to the cooling of Al/BL interface, as well. In fact, the cooling process occurred using circulating water as described in [43]. Briefly, water was first cooled to the different temperatures. Then, it was sprinkled onto the back side of the Al samples where Al substrate interfaces with the BL [43]. On the other hand, while the electrochemical cell was continuously stirred, its temperature was set to ~30 °C using circulating heating water.

In the second set, the pores in PAA were filled with just Fe (i.e., without Cu pre-plating) using the same Fe electrolyte conditions as mentioned above. It is obvious that, in this case, the branched-shape structures at the bottom of pores are also filled with Fe atoms. Figure 2 shows the fabrication
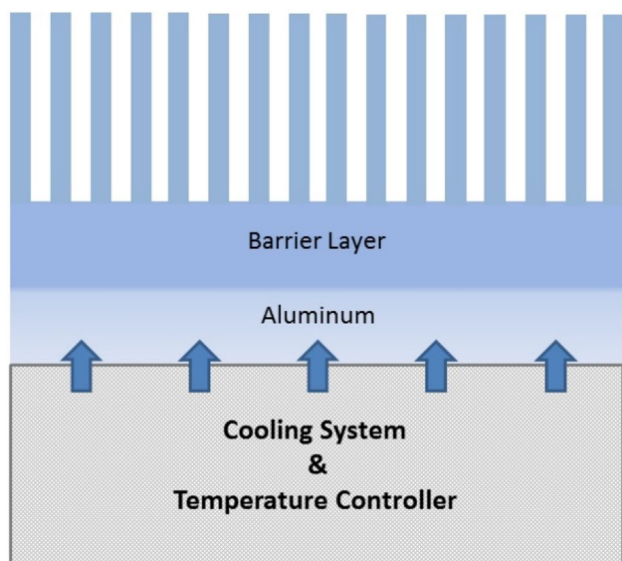
Fig. 1 Schematic of setup for controlling of BLT used in this study
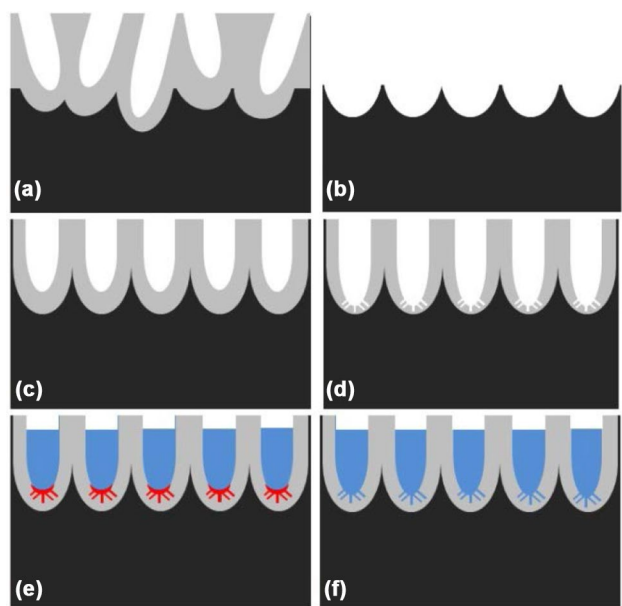

Fig. 2 Schematic diagram of PAA fabrication and electrodeposition of Fe NWs with/without Cu pre-plating: **a** first anodization in which the fabricated pores are disordered, **b** removal of oxide layer, **c** second anodization leading to highly ordered pores, **d** BL thinning process and creating branched-shape (tree-like) structures. Fabricating Fe NWs: **e** with Cu pre-plating and **f** without Cu pre-plating

of PAA with mild anodization (the two-step method) and electrodeposition of Fe NWs with/without Cu pre-plating.

Electrodeposition of Cu and Fe into the PAA was implemented by PED process. A sequence of pulses was applied using a precise modulated signal generator. Each pulse with the sine waveform had negative and positive polarities. The negative part is responsible for depositing metal inside the PAA pores (the reduction pulse). The positive pulse (the oxidation pulse) discharges the capacitance of the BL and interrupts the electric field at the deposition interface after each deposition pulse. It has been further reported that this pulse repairs discontinuities in the BL and improves its homogeneity [19]. Time duration between two pulses is called off-time (i.e., relaxation time) and was set to be 48 (ms) with $I = 0$ mA and $V = 0$ V. This slight time delay is helpful for repositioning Fe atoms and better crystallization, because a homogenous concentration along each nanopore before a new reduction pulse (the deposition pulse) is guaranteed. The current density for electrodeposition of Cu was chosen to be 25 or 35 mA/cm^2, while that of Fe electrodeposition was 25 mA/cm^2 [44]. In addition, the deposition charge was set to 2 °C for all NW samples.

The morphological properties of the PAA templates and Fe NWs were investigated by an atomic force microscope (AFM; NT-MDT) and a field-emission scanning electron microscope (FESEM; MIRA2 TESCAN). Fe NWs with/without Cu pre-plating in different BLTs were magnetically analyzed using a vibrating sample magnetometer (VSM; MDKB, Iran) at room temperature with a magnetic field applied parallel to the NWs' axis. To remove the remaining aluminum from NW samples, a saturated solution of copper sulfate and hydrochloric acid (CuCl$_2$) was initially diluted with distilled water (1:5 in volume) in a petri dish. Then, the Al substrate of NW samples was progressively dissolved in the solution during 1 h. Afterwards, X-ray diffraction (XRD) patterns were obtained by a Philips X-ray diffractometer using Ni-filtered Cu K$_\alpha$ radiation with $\lambda = 0.154$ nm.

3 Results and discussion

3.1 Morphological properties

Figure 3a shows a cross-sectional FESEM image of the PAA template with parallel nanopores. The inset shows a top-view atomic force microscope (AFM) image of the highly ordered nanopores with a diameter of approximately 35 nm after the second anodization. Moreover, the cross-sectional FESEM image of fabricated Fe NWs embedded in the PAA is shown in Fig. 3b. The diameter of each Fe NW is found to be about 35 nm and the length of NWs exceeds 2 μm.

Figure 4a shows voltage–time and current–time curves of the thinning process. This shows that the total process of BL thinning lasts about 1600 s. Consequently, with exponentially reducing voltage from 40 to 10 V [45], the passed current throughout the sample decreases from 4 to 0.5 mA. Figure 4b shows two sequential pulses with oxidation and reduction voltages and also off-time used in this study for depositing the metals inside PAA pores.
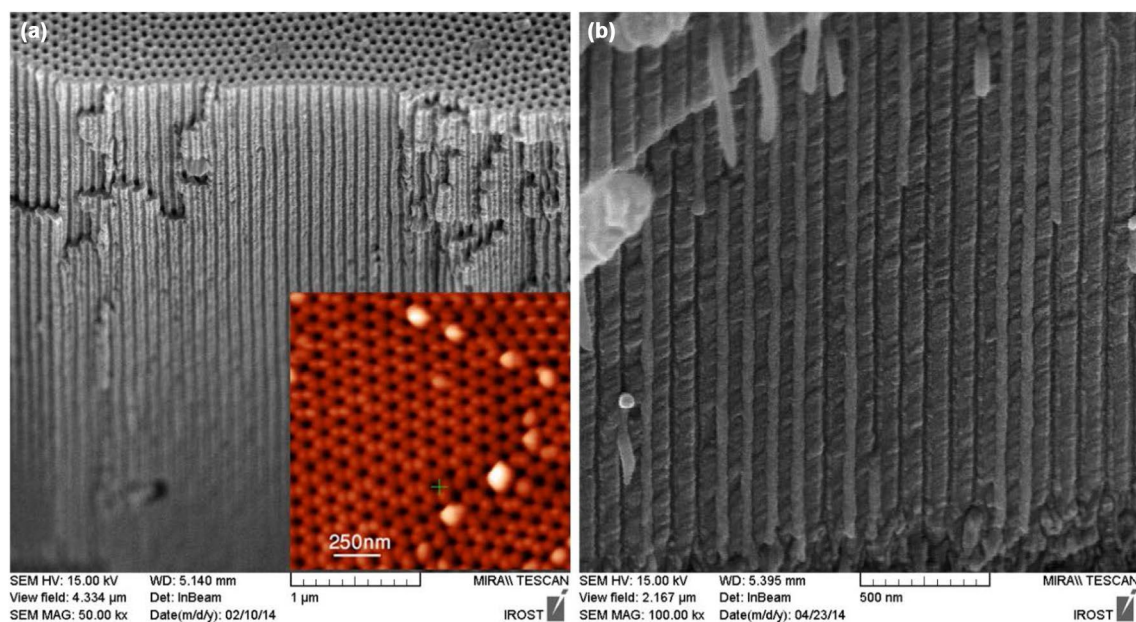
Fig. 3 **a** Cross-sectional FESEM image of the PAA template with a pore diameter of approximately 35 nm. The inset image shows a top-view AFM image of the highly ordered nanopores. **b** Cross-sectional FESEM view of Cu pre-plated Fe NWs embedded in PAA template
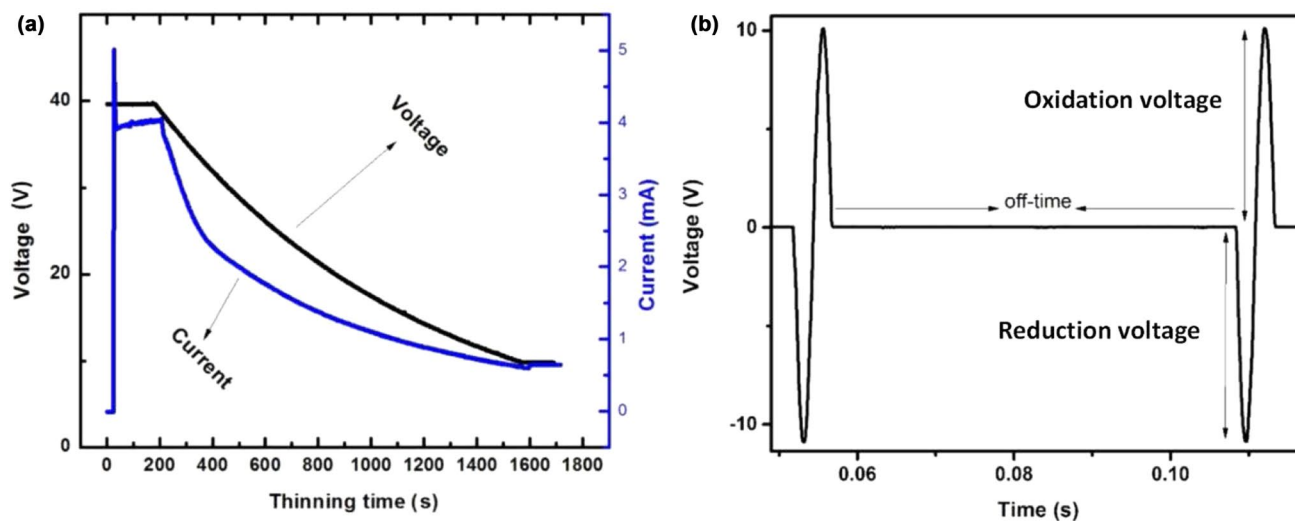

Fig. 4 **a** Voltage–time and current–time curves during the thinning process. The voltage is decreased exponentially from 40 to 10 V. **b** Applied sine waveform voltage versus time with off-time of 48 ms and reduction/oxidation voltage of 11/10 V in the electrodeposition process

3.2 Effect of pH at different BLTs on magnetic properties

The magnetic properties of Fe NWs fabricated in two pH regimes using BLTs of ~ 8, 16, and 24 °C were measured by VSM at room temperature. The corresponding hysteresis loops for Fe NWs without pre-plating at pH 2.6 and 4.0 using BLT ~ 24 °C are shown in Fig. 5. As can be seen, pH has a significant impact on the saturation magnetic moment value (M_s; in terms of emu [46]). Our results show that the

maximum M_s enhancement in the three different BLTs is obtained for the sample fabricated using BLT ~ 24 °C at pH 4.0, so that the increase is up to approximately 20 times compared to that of pH 2.6 (Fig. 5).

For a better understanding, a previously established approach was used to evaluate EE, providing insights from magnetic properties of NWAs. In fact, EE can be obtained through the ratio of actual amount of deposited magnetic material into the PAA (m_a) to that of expected amount (m_t) [31]. In this study, m_a was obtained based on magnetometry.
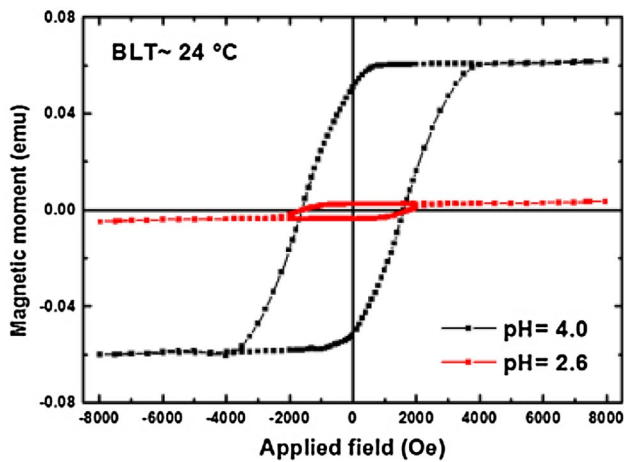
Fig. 5 Hysteresis loops of Fe NWs without Cu pre-plating fabricated in the electrolyte with pH values of 2.6 and 4.0 using BLT ~ 24 °C

In other words, by comparing M_s (in terms of emu) with the saturation magnetization of Fe NWs (~ 180 emu/g [47]), m_a (g) is found to be: $m_a(g) = \frac{M_s(\text{emu})}{180 \text{ emu/g}}$.

On the other hand, since the deposited charge was constant to 2C for all samples, m_t is found to be approximately 1.04×10^3 mol or 5.808×10^{-4} g for Fe NW samples. As mentioned before, the exposed deposition area was kept constant, thereby making a reasonable comparison. In Table 1, EE% and magnetic properties (including coercivity H_c and remanence ratio M_r/M_s) are represented for the Fe NW samples without Cu pre-plating. As seen, m_a increases with increasing pH while also enhancing EE%. It is well known that, for higher pH values, the hydrogen concentration becomes smaller. In turn, this may cause the deposition possibility of Fe ions in competition with hydrogen ions to be increased, thus improving the growth rate of NWs [44].

From magnetic properties' point of view, the resulting 35 nm-diameter-electrodeposited Fe NWAs with a few microns in length in this study have considerably higher H_c (ranging between 1600 and 1800 Oe) and M_r/M_s (~ 0.8−0.9) than those of obtained in the recent reports [47–49]. For example, using a DC electrodeposition method followed by

Table 1 Fabrication and magnetic parameters for Fe NW samples without Cu pre-plating in two pH regimes

BLT (°C)	pH	m_a (μg)	EE%	H_c (Oe)	M_r/M_s
~ 8	4	326	56.21	1640	0.792
	2.6	73.1	12.58	1590	0.915
~ 16	4	323	55.62	1590	0.803
	2.6	57.4	9.87	1530	0.857
~ 24	4	349	60.09	1610	0.821
	2.6	15.7	2.7	1820	0.826

an annealing process, Fe NWs with maximum H_c and M_r/M_s of 576 Oe and 0.18 were fabricated into the PAA template [48]. By a combination of electrospinning and sol–gel processes, Han et al. [49] synthesized Fe NWs with diameters between 30 and 40 nm, thereby obtaining $H_c = 479$ Oe. Moreover, Goncharova et al. [47] fabricated oriented arrays of Fe NWs with a diameter of approximately 40 nm and a length of up to a few dozens of microns via an electrodeposition process into the PAA template. In this case, H_c was found to be 815 Oe despite the polycrystalline structure of the Fe NWs. Consequently, the higher H_c measured in the present study may indicate the fabrication of highly crystalline Fe NWAs, enhancing the magnetocrystalline anisotropy [50]. Alternatively, it is worth noting that, while magnetic properties of the Fe NWAs remain almost similar as a function of pH, EE% significantly increases when increasing pH. Based on a previous report [36], changing the fabrication parameters led to significant variations in H_c of Fe NWs. In this regard, increasing the deposition frequency from 50 to 700 Hz enhanced H_c from 1010 to 1810 Oe [36]. Therefore, regardless of fabrication parameters (including BLT and pH), the constant trend of magnetic properties in this study may be a helpful feature, providing applicability in the fabrication of perpendicular magnetic data storage devices [51].

3.3 Effect of BLT variation on electrodeposition efficiency (EE)

As indicated in the previous section, M_s increased up to 20 times when using the electrolyte with pH 4.0 compared to that of pH 2.6. Herein, the effect of BLT variation on M_s of Fe NW samples has been investigated at pH 4.0. In this regard, BLT was changed from ~ 4 to ~ 32 °C while the electrolyte temperature was fixed to ~ 30 °C. In Fig. 6, M_s as a function of BLT is demonstrated, indicating that under the same electrochemical conditions, BLT has a considerable
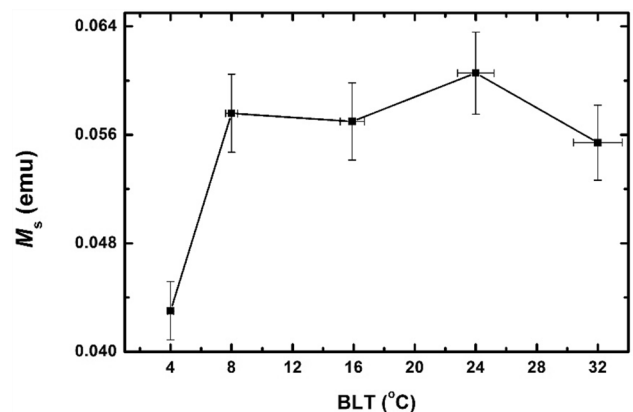

Fig. 6 Saturation magnetic moment (M_s) of Fe NW samples without Cu pre-plating as a function of BLT at pH 4.0

effect on M_s of NW samples. In other words, increasing BLT from ~ 4 to ~ 24 °C increases M_s up to approximately 45%, thereby enhancing the corresponding EE.

Therefore, according to Table 2, the maximum EE% in the fabrication of Fe NWAs was found to be about 60% when there is a 6 °C temperature difference between BLT and the electrolyte temperature. This result distinguishes between this study and a recent report in which the optimum electrolyte temperature was found to be ~ 12 °C (according to Einstein–Stokes equation) for highly homogeneous filled PAA templates [22]. In this regard, for electrolyte temperatures below 5 °C, solution precipitation occurred, thereby covering the PAA template and inhibiting the electrodeposition [32]. Alternatively, for electrolyte temperatures above 40 °C, strong hydrogen evolution hindered the electrodeposition of Fe NWs, thereby decreasing the filling percentage [32]. Thus, our proposed approach is capable of providing a high EE up to 60% for electrodepositing Fe NWs in the PAA templates based on the low temperature difference.

To understand the mechanism of BLT effect, we take into account pulse conditions during the electrodeposition process. According to the literature [51, 52], the oxide layer

induced during the anodization (i.e., the BL) can act as a semiconductor and has rectifying features, thereby enabling us to use AC pulses in the electrodeposition [52, 53].

Figure 7 shows voltage–time and current–time curves simultaneously recorded during the electrodeposition process. These pulses were applied in sequence for the electrodeposition of Fe NWs. In an AC pulse, the current is expected to increase when enhancing the voltage. However, the BL represents resistance to the current increase due to its rectifying feature. This can be manifested at the onset of reduction voltage pulse. In this respect, while Fig. 7a shows a weak BL behavior for the NW sample fabricated using BLT ~ 4 °C, Fig. 7b indicates a typical BL when using BLT ~ 24 °C for electrodepositing Fe NWs. In this way, the variation behavior of EE follows that of BL when using BLT ~ 4 and 24 °C (see Table 2).

3.4 Effect of Cu pre-plating

As known, the precise control of BL and electrodeposition in branched nanopores is of extreme importance [54, 55]. According to Sect. 3.1, reaching a high M_s (thus corresponding to a high EE) in the fabrication of Fe NWAs at pH 2.6 presents a challenge. Herein, we investigated the effect of Cu pre-plating at the bottom of PAA pores on M_s of Fe NW samples using BLT ~ 8, 16, and 24 °C at pH 2.6 and 4.0. Initially, however, the effect of two different current densities ($j = 25$ and 35 mA/cm^2) on M_s of NW samples was also investigated for Cu pre-plated Fe NWs.

Figure 8 shows hysteresis loops of Fe NW samples fabricated with/without Cu pre-plating process using BLT ~ 8 °C and $j = 25$ and 35 mA/cm^2 in two pH regimes. As inferred, while the Cu pre-plating and current density have no considerable effect on M_s at pH 4.0, the Cu

Table 2 Electrodeposition efficiency (EE) and magnetic properties of Fe NW samples without Cu pre-plating as a function of BLT at pH 4.0

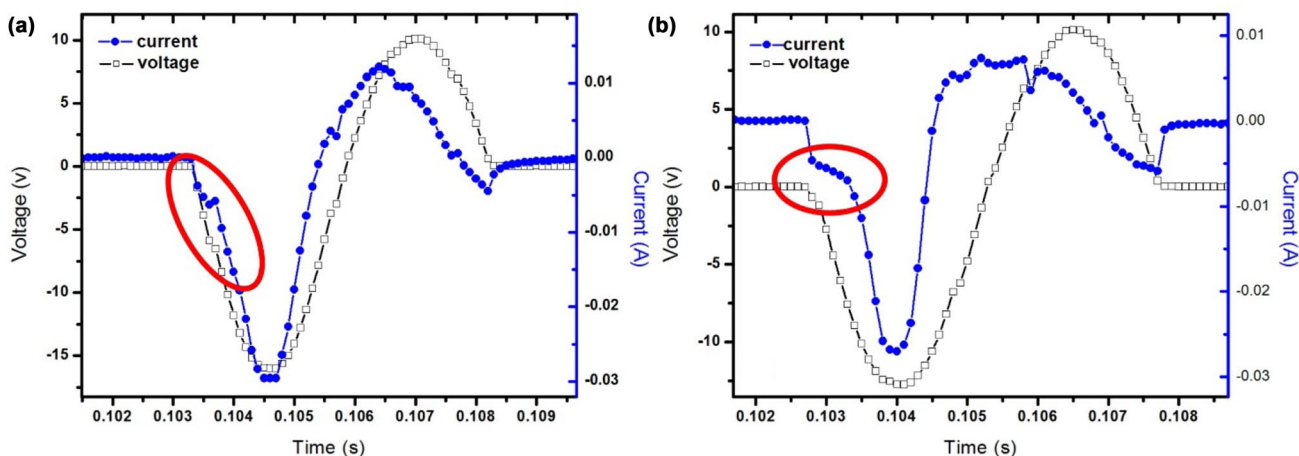| BLT (°C)	EE%	H_c (Oe)	M_r/M_s
~ 4	42.1	1660	0.7905
~ 8	56.21	1640	0.792
~ 16	55.62	1590	0.803
~ 24	60.09	1610	0.821
~ 32	54.21	1650	0.85

Fig. 7 Voltage–time and current–time curves recorded during the electrodeposition of Fe NWs using pH 4.0: **a** BLT ~ 4 °C and **b** BLT ~ 24 °C. The marked areas show the onset of reduction voltage pulse
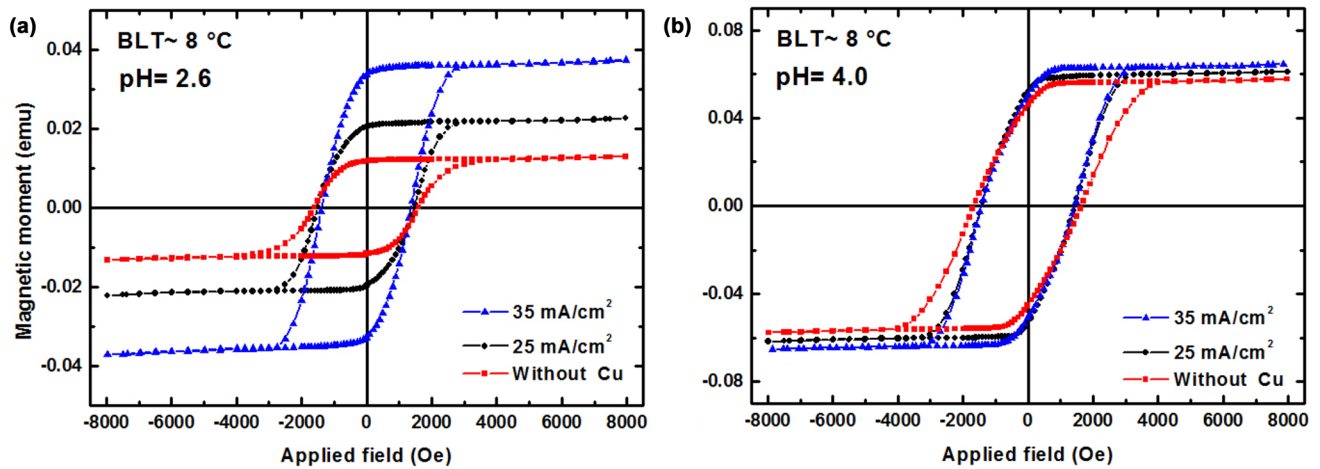
Fig. 8 Hysteresis loops of Fe NW samples fabricated with/without Cu pre-plating process using BLT ~ 8 °C and $j = 25$ and 35 mA/cm^2 at pH values of **a** 2.6 and **b** 4.0

pre-plated Fe NW sample fabricated at pH 2.6 has an enhanced M_s of up to 70%. In this case, increasing the current density to 35 mA/cm^2 has further increased M_s compared to that of using $j = 25$ mA/cm^2 (see Fig. 8a). Therefore, apart from the current density, performing the Cu pre-plating at the branched nanopores could provide an improved EE in the fabrication of Fe NWs at pH 2.6. It is worth noting that, according to Table 1, the electrodeposition of Fe NWs at the lower pH value was hindered in different BLTs, most likely due to the hydrogen evolution and BL breakdown [32]. Thus, using the Cu pre-plating may improve the performance and durability of BL when electrodepositing Fe NWs as evidenced with the higher M_s (Fig. 8a). On the other hand, the increase in current density up to 35 mA/cm^2 in the Cu pre-plated samples can provide finer nucleation sites for the subsequent

electrodeposition of Fe NWs, thus limiting the hydrogen evolution and enhancing M_s [56].

Using the current density of 35 mA/cm^2, Fig. 9 evidences the effect of BLT on magnetic properties of Cu pre-plated Fe NW samples at pH 2.6 and 4.0. Noticeably, M_s considerably increases with reducing BLT regardless of pH value, so that it is maximized for BLT ~ 8 °C. Therefore, it may be stated that the cooling of BL in Cu pre-plated samples has nearly neutralized pH involvement in M_s, giving rise to an efficient electrodeposition without BL breakdown at the lower pH value.

3.5 XRD analysis

Figure 10 depicts the XRD patterns of Cu pre-plated Fe NWAs fabricated using BLT ~ 8 °C in the two pH regimes.
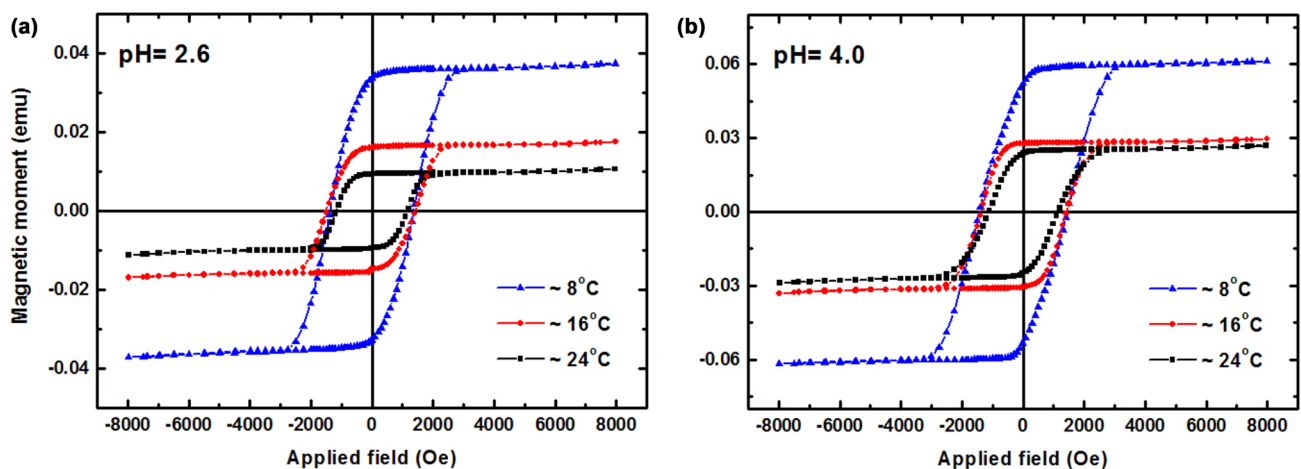

Fig. 9 Hysteresis loops of Cu pre-plated Fe NW samples fabricated using BLT ~ 8, 16, and 24 °C for **a** pH 2.6 and **b** pH 4.0
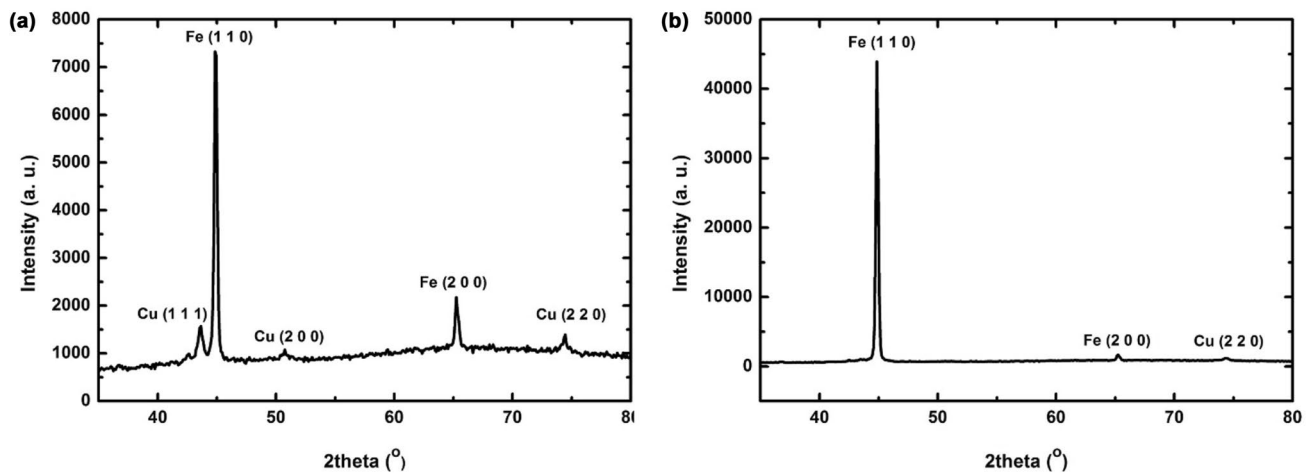
Fig. 10 XRD patterns of Cu pre-plated Fe NW samples fabricated using BLT ~ 8 °C at pH values of **a** 2.6 and **b** 4.0

As observed, both samples show a *bcc*-Fe structure oriented along the [110] direction, indicating highly crystalline Fe NWs. Most of the earlier reports on Fe NWs were focused on the shape anisotropy as a key factor in magnetic properties [57, 58]. In other words, more attention should be paid to crystalline properties of Fe NWs by which to reinforce the total anisotropy. In this respect, the easy direction for single crystals of Fe is along [100]. In most cases; however, the preferential direction of Fe NWs is [110], so that the ratio of (110) to (200) peak is very high [36, 54, 59–61]. Therefore, efforts have been on the increase of (200) peak intensity, which can provide applications in nanosensors and perpendicular high-density recording media [29]. Here, (200)/(110) ratio has increased from 3.81 to 30.04% when decreasing pH from 4.0 to 2.6. Furthermore, using Scherrer's equation [35], the mean crystallite size was estimated along the crystallographic planes. It was found that, while the crystallite size along the [110] direction decreases from approximately 37.5 nm (pH 4.0) to 31.5 nm (pH 2.6), it remains almost constant to 25.5 nm along the [100] direction. It should be noted that *fcc*-Cu reflections including Cu(111), Cu(200), and Cu(220) in the XRD patterns indicate the presence of branched nanopores filled with Cu.

4 Conclusions

In conclusion, highly ordered Fe NWs (exceeding 2 μm in length) were fabricated in PAA templates using the pulsed electrodeposition method. We performed a study on the influence of BL conditions including BLT (ranging between ~ 4 and 32 °C) and Cu pre-plating at the dendritic sections of pores on EE and magnetic properties of Fe NWAs in two pH regimes (2.6 and 4.0). For the pH value of 4.0, a maximum EE of 60% was obtained using BLT ~ 24 °C in the fabrication of Fe NWs without Cu pre-plating. In the case of pH 2.6, we found low EEs (< 13%) which were improved up to 40% after performing the Cu pre-plating and avoiding BL breakdown. Hysteresis loops showed a nearly constant trend of magnetic properties under different fabrication parameters, arising from a *bcc*-Fe structure highly oriented along [110] direction.

Compliance with Ethical Standards

By submitting the manuscript, the authors understand that the material presented in this manuscript has not been published before, nor has it been submitted for publication to another journal. The corresponding author attests that this study has been approved by all the co-authors concerned.

Conflict of interest The authors declare that they have no conflict of interest.

References

1. Q. Liu, C. Gao, J. Xiao, D. Xue, Size effects on magnetic properties in Fe$_{0.68}$ Ni$_{0.32}$ alloy nanowire arrays, J. Magn. Magn. Mater. **260**, 151–155 (2003).
2. P.D. McGary, L. Tan, J. Zou, B.J. Stadler, P.R. Downey, A.B. Flatau, Magnetic nanowires for acoustic sensors. J. Appl. Phys. **99**, 08B310 (2006)
3. M. Vázquez, Soft magnetic wires. Physica B **299**, 302–313 (2001)
4. V. Haehnel, S. Fähler, P. Schaaf, M. Miglierini, C. Mickel, L. Schultz, H. Schlörb, Towards smooth and pure iron nanowires grown by electrodeposition in self-organized alumina membranes. Acta Mater. **58**, 2330–2337 (2010)

5. J. Smyth, S. Schultz, D. Kern, H. Schmid, D. Yee, Hysteresis of submicron permalloy particulate arrays. J. Appl. Phys. **63**, 4237–4239 (1988)

6. J. Wong, A. Scherer, M. Todorovic, S. Schultz, Fabrication and characterization of high aspect ratio perpendicular patterned information storage media in an Al_2O_3/GaAs substrate. J. Appl. Phys. **85**, 5489–5491 (1999)

7. P. Vavassori, V. Metlushko, B. Grimsditch, B. Ilic, P. Neuzil, R. Kumar, Magneto-optical studies of superlattice dot arrays. Phys. Rev. B **61**, 5895 (2000)

8. C. Moreau, J. Caballero, R. Loloee, W. Pratt Jr., N.O. Birge, Fabrication and magnetic characterization of single domain $Co_{91}Fe_9$ nanostructures. J. Appl. Phys. **87**, 6316–6318 (2000)

9. F. Rousseaux, D. Decanini, F. Carcenac, E. Cambril, M. Ravet, C. Chappert, N. Bardou, B. Bartenlian, P. Veillet, Study of large area high density magnetic dot arrays fabricated using synchrotron radiation based X-ray lithography. J. Vac. Sci. Technol. B **13**, 2787–2791 (1995)

10. C. Pike, A. Fernandez, An investigation of magnetic reversal in submicron-scale Co dots using first order reversal curve diagrams. J. Appl. Phys. **85**, 6668–6676 (1999)

11. A. Fernandez, M. Gibbons, M. Wall, C. Cerjan, Magnetic domain structure and magnetization reversal in submicron-scale Co dots. J. Magn. Magn. Mater. **190**, 71–80 (1998)

12. L. Kong, L. Zhuang, M. Li, B. Cui, S.Y. Chou, Fabrication, writing, and reading of 10 Gbits/in2 longitudinal quantized magnetic disks with a switching field over 1000 Oe. Jpn. J. Appl. Phys. **37**, 5973–5975 (1998)

13. Y.M. Cho, W.K. Choo, H. Kim, D. Kim, Y. Ihm, Effects of rapid thermal annealing on the ferromagnetic properties of sputtered $Zn_{1-x}(Co_{0.5}Fe_{0.5}) \times O$ thin films. Appl. Phys. Lett. **80**, 3358–3360 (2002)

14. S. Wirth, S. Von Molnar, M. Field, D. Awschalom, Magnetism of nanometer-scale iron particles arrays. J. Appl. Phys. **85**, 5249–5254 (1999)

15. C.R. Martin, Membrane-based synthesis of nanomaterials. Chem. Mater. **8**, 1739–1746 (1996)

16. J. Montero-Moreno, M. Belenguer, M. Sarret, C. Müller, Production of alumina templates suitable for electrodeposition of nanostructures using stepped techniques. Electrochim. Acta **54**, 2529–2535 (2009)

17. H. Asoh, S. Ono, T. Hirose, M. Nakao, H. Masuda, Growth of anodic porous alumina with square cells. Electrochim. Acta **48**, 3171–3174 (2003)

18. I. Vrublevsky, A. Jagminas, J. Schreckenbach, W.A. Goedel, Electronic properties of electrolyte/anodic alumina junction during porous anodizing. Appl. Surf. Sci. **253**, 4680–4687 (2007)

19. K. Nielsch, F. Müller, A.-P. Li, U. Gösele, Uniform nickel deposition into ordered alumina pores by pulsed electrodeposition. Adv. Mater. **12**, 582–586 (2000)

20. M. Michalska-Domańska, M. Norek, W.J. Stępniowski, B. Budner, Fabrication of high quality anodic aluminum oxide (AAO) on low purity aluminum—a comparative study with the AAO produced on high purity aluminum. Electrochim. Acta **105**, 424–432 (2013)

21. C. Sousa, D. Leitao, M. Proenca, A. Apolinario, J. Correia, J. Ventura, J. Araujo, Tunning pore filling of anodic alumina templates by accurate control of the bottom barrier layer thickness. Nanotechnology **22**, 315602 (2011)

22. J. Azevedo, C. Sousa, J. Ventura, A. Apolinario, A. Mendes, J. Araujo, Ultra-long Fe nanowires by pulsed electrodeposition with full filling of alumina templates. Mater. Res. Express **1**, 015028 (2014)

23. W. Cheng, M. Steinhart, U. Gösele, R.B. Wehrspohn, Tree-like alumina nanopores generated in a non-steady-state anodization. J. Mater. Chem. **17**, 3493–3495 (2007)

24. M. Ghaffari, A. Ramazani, M.A. Kashi, Improvement in the microstructure and magnetic properties in arrays of dc pulse electrodeposited Co nanowires induced by Cu pre-plating. J. Phys. D Appl. Phys. **46**, 295002 (2013)

25. A. Yin, J. Li, W. Jian, A. Bennett, J. Xu, Fabrication of highly ordered metallic nanowire arrays by electrodeposition. Appl. Phys. Lett. **79**, 1039–1041 (2001)

26. M. Sun, G. Zangari, R.M. Metzger, Cobalt island arrays with in-plane anisotropy electrodeposited in highly ordered alumite. IEEE Trans. Magn. **36**, 3005–3008 (2000)

27. M.S. Salem, P. Sergelius, R. Zierold, J.M.M. Moreno, D. Görlitz, K. Nielsch, Magnetic characterization of nickel-rich NiFe nanowires grown by pulsed electrodeposition. J. Mater. Chem. **22**, 8549–8557 (2012)

28. S. Krimpalis, O.-G. Dragos, A.-E. Moga, N. Lupu, H. Chiriac, Magnetization processes in electrodeposited NiFe/Cu multilayered nanowires. J. Mater. Res. **26**, 1081–1090 (2011)

29. H. Hu, H. Chen, J. Chen, G. Wu, Magnetic properties of (110)-and (200)-oriented Fe-nanowire arrays. Phys. B **368**, 100–104 (2005)

30. A. Ramazani, M.A. Kashi, M. Alikhani, S. Erfanifam, Optimized microstructure and magnetic properties in arrays of ac electrodeposited Co nanowires induced by the continuous and pulse electrodeposition. J. Phys. D Appl. Phys. **40**, 5533 (2007)

31. K.M. Razeeb, F.M. Rhen, S. Roy, Magnetic properties of nickel nanowires: effect of deposition temperature. J. Appl. Phys. **105**, 083922 (2009)

32. A. Rashidi, A. Amadeh, The effect of current density on the grain size of electrodeposited nanocrystalline nickel coatings. Surf. Coat. Technol. **202**, 3772–3776 (2008)

33. C. Cui, B. Wang, W. Yang, J. Sun, Effect of deposition voltage and Co^{2+} concentration on the texture and magnetic properties of Co nanowire arrays, J. Crystal Growth **324**, 168–171 (2011)

34. M. Almasi Kashi, A. Ramazani, M. Ghaffari, V. Isfahani, The effect of growth rate enhancement on the magnetic properties and microstructures of ac electrodeposited Co nanowires using non-symmetric reductive/oxidative voltage. J. Cryst. Growth **311**, 4581–4586 (2009)

35. J. Azevedo, C. Sousa, A. Mendes, J. Araújo, Influence of the rest pulse duration in pulsed electrodeposition of Fe nanowires. J. Nanosci. Nanotechnol. **12**, 9112–9117 (2012)

36. A. Ramazani, M.A. Kashi, V.B. Isfahani, M. Ghaffari, The influence of crystallinity enhancement on the magnetic properties of ac electrodeposited Fe nanowires. Appl. Phys. A **98**, 691–697 (2010)

37. D. Leitao, A. Apolinario, C. Sousa, J. Ventura, J. Sousa, M. Vazquez, J. Araujo, Nanoscale topography: a tool to enhance pore order and pore size distribution in anodic aluminum oxide. J. Phys. Chem. C **115**, 8567–8572 (2011)

38. M. Almasi Kashi, A. Ramazani, A. Esmaeily, Magnetostatic interaction investigation of CoFe alloy nanowires by first-order reversal-curve diagrams. IEEE Trans. Magn. **49**, 1167–1171 (2013)

39. Y. Sui, B. Cui, L. Martınez, R. Perez, D.J. Sellmyer, Pore structure, barrier layer topography and matrix alumina structure of porous anodic alumina film. Thin Solid Films **406**, 64–69 (2002)

40. K. Nielsch, J. Choi, K. Schwirn, R.B. Wehrspohn, U. Gösele, Self-ordering regimes of porous alumina: the 10 porosity rule. Nano Lett. **2**, 677–680 (2002)

41. D.V. Kumar, S. Ayyagari, M. Prasad, Mechanical characteristics and electrochemical behaviour of electrodeposited nanocrystalline iron and iron-nickel alloy. Mater. Chem. Phys. **201**, 26–34 (2017)

42. F.E. Atalay, H. Kaya, S. Atalay, S. Tari, Influences of deposition time and pH on magnetic NiFe nanowires fabrication. J. Alloy. Compd. **469**, 458–463 (2009)

43. M. Noormohammadi, M. Moradi, Structural engineering of nanoporous alumina by direct cooling the barrier layer during the aluminum hard anodization. Mater. Chem. Phys. **135**, 1089–1095 (2012)

44. H. Venkatasetty, Electrodeposition of thin magnetic permalloy films. J. Electrochem. Soc. **117**, 403–407 (1970)

45. A. Montazer, A. Ramazani, M. Almasi, Kashi, Magnetically extracted microstructural development along the length of Co nanowire arrays: The interplay between deposition frequency and magnetic coercivity. J. Appl. Phys. **120**, 113902 (2016)

46. C. Sousa, D. Leitao, M. Proença, A. Apolinário, A. Azevedo, N. Sobolev, S. Bunyaev, Y.G. Pogorelov, J. Ventura, J. Araujo, Probing the quality of Ni filled nanoporous alumina templates by magnetic techniques. J. Nanosci. Nanotechnol. **12**, 7486–7490 (2012)

47. A.S. Goncharova, S.V. Sotnichuk, A.S. Semisalova, T.Y. Kiseleva, I. Sergueev, M. Herlitschke, K.S. Napolskii, A.A. Eliseev, Oriented arrays of iron nanowires: synthesis, structural and magnetic aspects., J. Sol Gel. Sci. Technol. **81**, 1–6 (2016)

48. M. Irfan, U. Khan, W. Li, N. Adeela, K. Javed, X. Han, Magnetic investigations of post-annealed metallic Fe nanowires via electro-deposition method. Mater. Lett. **180**, 235–238 (2016)

49. R. Han, W. Li, W. Pan, M. Zhu, D. Zhou, F.-s. Li, 1D magnetic materials of Fe_3O_4 and Fe with high performance of microwave absorption fabricated by electrospinning method. Sci. Rep. **4**, 7493 (2014)

50. B.D. Cullity, C.D. Graham, Introduction to magnetic materials (John Wiley & Sons, New Jersey 2011)

51. X. Huang, L. Li, X. Luo, X. Zhu, G. Li, Orientation-controlled synthesis and ferromagnetism of single crystalline Co nanowire arrays. J. Phys. Chem. C **112**, 1468–1472 (2008)

52. J. Xu, K. Wang, Pulsed electrodeposition of monocrystalline Ni nanowire array and its magnetic properties. Appl. Surf. Sci. **254**, 6623–6627 (2008)

53. D. AlMawlawi, N. Coombs, M. Moskovits, Magnetic properties of Fe deposited into anodic aluminum oxide pores as a function of particle size. J. Appl. Phys. **70**, 4421–4425 (1991)

54. G. Sharma, M.V. Pishko, C.A. Grimes, Fabrication of metallic nanowire arrays by electrodeposition into nanoporous alumina membranes: effect of barrier layer. J. Mater. Sci. **42**, 4738–4744 (2007)

55. C.T. Sousa, A. Apolinario, D.C. Leitao, A.M. Pereira, J. Ventura, J.P. Araujo, Precise control of the filling stages in branched nano-pores. J. Mater. Chem. **22**, 3110–3116 (2012)

56. A.J. Bard, L.R. Faulkner, Electrochemical methods: fundamentals and applications (Wiley, New York, 1980)

57. X. Zhang, G. Wen, Y. Chan, R. Zheng, X. Zhang, N. Wang, Fabrication and magnetic properties of ultrathin Fe nanowire arrays. Appl. Phys. Lett. **83**, 3341–3343 (2003)

58. S. Yang, H. Zhu, D. Yu, Z. Jin, S. Tang, Y. Du, Preparation and magnetic property of Fe nanowire array. J. Magn. Magn. Mater. **222**, 97–100 (2000)

59. M. Ou, T. Yang, Y. Chen, Anisotropic magnetism and magne-toresistance in iron nanowire arrays. Chin. J. Phys. **47**, 848–853 (2009)

60. X. Wang, C. Li, G. Chen, C. Peng, L. He, L. Yang, Synthesis and characterization of Fe nanowire arrays by AC electrodeposition in PAMs. Surf. Rev. Lett. **17**, 419–423 (2010)

61. J.B. Wang, X.Z. Zhou, Q.F. Liu, D.S. Xue, F.S. Li, B. Li, H.P. Kunkel, G. Williams, Magnetic texture in iron nanowire arrays. Nanotechnology **15**, 485 (2004)